Luminescence line-shape analysis of the electron-hole plasma in direct-gap Ga-Al-As: Random-phase-approximation approach

A. Selloni, S. Modesti, and M. Capizzi
Dipartimento di Fisica, Università degli Studi di Roma "La Sapienza," Piazzale Aldo Moro 2, I-00185 Roma, Italy
(Received 23 January 1984)

The luminescence line shapes of an electron-hole plasma in Ga-Al-As have been calculated within the random-phase approximation (RPA). Different models have been tested for the spectral weight function. The fully self-consistent RPA is found to overestimate the weight of the plasmon sideband and to underestimate the energy-gap narrowing. An approach which neglects plasmon replicas instead yields luminescence spectra in excellent agreement with experiment over a wide range of plasma densities and temperatures. A further model is also introduced to estimate an upper bound for the weight of plasmon sidebands in the experimental spectra. We used both static and dynamical phonon screening. We found that the former screening correctly describes luminescence up to densities such that the plasmon energy is of the order of the longitudinal-optical-phonon energy.

I. INTRODUCTION

The experimental achievement of three-dimensional confinement has allowed the study of a uniform electron-hole plasma (EHP) in Ga-Al-As for a wide range of densities.[1,2] This technique avoids the necessity of additional models to account for the EHP expansion[3,4] and the ensuing drift phenomena.[5]

In a previous paper,[2] the measured luminescence spectra from a uniform EHP were analyzed in terms of a phenomenological model, similar to that used by Martin and Störmer.[6] Neglecting electron-hole interactions, luminescence was treated as being due to direct, k-conserving transitions between single-particle electron and hole states. The broadening of these states caused by many-body interactions was explicitly evaluated within the random-phase approximation (RPA), while the renormalization of single-particle energies was assumed to be a constant, determined at each density by fitting the experimental band position. The model was found to fit rather well the overall experimental luminescence line shapes over a large range of EHP densities and aluminum concentrations. Some misfit, on the low-energy side of the spectra, was tentatively attributed to the neglect of plasmon replica contributions. The extracted values of the renormalized energy gap E_G' were found to be in close agreement with the values resulting from the theory of Vashishta *et al.*[7] for nonpolar materials.

In this paper we are concerned with a detailed study of many-body interactions in the EHP luminescence at various densities and temperatures. We shall attempt a complete self-consistent RPA description of the EHP luminescence, also including—besides broadening effects—the renormalization of single-particle energies and plasmon replica contributions. A quantitative test of the theory, in particular of the importance of "beyond-RPA" interactions, will be provided by direct comparison to experiment.

Assuming k conservation and a constant optical matrix element M, we start by expressing the luminescence intensity $I(\omega)$ in the form

$$I(\omega)=|M|^2\int d^3k\int d\omega_e d\omega_h A_e(k,\omega_e)A_h(k,\omega_h) \times F_e(\omega_e)F_h(\omega_h)\delta(\omega-\omega_e-\omega_h)\ , \tag{1}$$

where A_e and A_h are the spectral weight functions for the electrons and holes, respectively, and F_e and F_h the corresponding Fermi functions. Equation (1) is then interpreted as follows. The electron-hole (e-h) recombination process amounts to creating an electron in the system of the holes and a hole in the system of the electrons. $A_h(k,\omega_h)$ [$A_e(k,\omega_e)$] gives the probability that the hole (electron) system is left in an excited state of momentum k and energy ω_h (ω_e).[8] The luminescence intensity at energy ω is given by the convolution of the two probabilities, as given by Eq. (1), if we assume that these are independent. In other words, Eq. (1) accounts for the energy renormalization and finite lifetime (self-energy corrections) of single-particle states, but neglects the electron-hole interaction (vertex corrections). This term was evaluated for the gain spectrum of GaAs (Ref. 9) and Ge (Ref. 10) and found to cause a strong reduction of the plasmon sideband with respect to the case where only self-energy corrections were included. Interactions with plasmons are indeed weaker in recombination processes, which maintain charge neutrality.[11] However, the approach of Brinkman and Lee cannot be immediately extended to the EHP densities achieved in our experiment, because divergencies can occur.[9,12] In this paper we restrict ourselves to self-energy corrections, while the importance of vertex corrections will be evaluated indirectly.

Our discussion will be articulated in various steps, corresponding to different models for the spectral functions. In all cases the self-energy $\Sigma(k,\omega)$ is evaluated to lowest order in the dynamically screened interaction (RPA). We shall start with the fully self-consistent calculation, in which $A_{e,h}(k,\omega)$ are given by[8]

$$A_{e,h}(k,\omega)=\pi^{-1}\mathrm{Im}[\omega-e_{e,h}(k)-\Sigma_{e,h}(k,\omega)]^{-1}\ , \tag{2}$$

where $e_{e,h}(k)$ are the electron and hole energies in the absence of interactions (model 1). The resulting luminescence line shapes are found to significantly overestimate the plasmon sideband. Moreover the exchange-correlation contribution to the chemical potential (i.e., the band-gap renormalization $\Delta E_G = E_G - E_G'$) turns out to be too small in comparison with the values predicted by more complete theories.[7] The other two models—which give an alternative representation of the spectral functions—do not have a rigorous justification: They are introduced with the main purpose of quantitatively estimating the weight of plasmon replicas in the experimental spectra. For the second model we follow an early suggestion by Rice[13] and evaluate the self-energy at the independent-particle energy $\omega = e_{e,h}(k)$, so that the spectral functions reduce to simple Lorentzians and plasmon replicas are completely suppressed. The experimental luminescence line shapes and energy positions are fitted very well, although some residual difficulties are left (discussed in detail in Secs. II and III). Finally, in the third model the full ω dependence of the imaginary part of the self-energy is retained in the spectral functions, while $\mathrm{Re}\Sigma_{e,h}$ is evaluated at $\omega = e_{e,h}(k)$. In this approximation, which is often employed to describe EHP gain spectra,[14] the plasmon sidebands are strongly reduced with respect to the fully self-consistent case. Line shapes are again quite well reproduced, while a misfit in the energy positions is found.

The last issue of this work is to compare the static and dynamical phonon screening. It is commonly believed that the dynamical screening should be used at high densities.[15,16] Beni and Rice[15] found that in low-polar materials, like GaAs, the static screening works better than the dynamical one whenever the plasma frequency ω_p is much smaller than the longitudinal-optical (LO) phonon frequency ω_l. We found that the static approximation works actually well up to EHP densities such that $\omega_p \sim \omega_l$. Results obtained in both approximations are substantially identical. Most of our results and discussions will be referred to the static model.

This paper is organized as follows. In Sec. II we describe the calculation of the self-energy and spectral weight functions. The static and dynamical phonon screening approximations are discussed in Secs. II A and II B, respectively. Luminescence line shapes are compared to experiment in Sec. III. Concluding remarks are given in Sec. IV.

II. CALCULATIONS

A. The self-energy and the spectral weight function static phonon screening

When a particle with wave vector k is added to an interacting, uniform N-particle system, the probability density of finding the $(N+1)$-particle system excited to an energy ω is given by the spectral weight function[8] [see Eq. (2)]

$$A_{e,h}(k,\omega) = \pi^{-1} \frac{|\Sigma_I^{e,h}(k,\omega)|}{|\omega - e_{e,h}(k) - \Sigma_R^{e,h}(k,\omega)|^2 + |\Sigma_I^{e,h}(k,\omega)|^2} , \tag{3}$$

where $\Sigma_R^{e,h}$ and $\Sigma_I^{e,h}$ are the real and imaginary parts of the self-energy Σ and $e_{e,h}(k)$ are the independent-particle dispersion relations. Since the conduction-band minimum of Ga-Al-As is isotropic and nondegenerate, we have $e_e(k) = \hbar^2 k^2 / 2m_e$ for electrons. Close to the top of the valence bands we approximate the hole dispersion by $e_h(k) = \hbar^2 k^2 / 2m_{dh}$, where $m_{dh} = (m_{\mathrm{hh}}^{3/2} + m_{\mathrm{lh}}^{3/2})^{2/3}$ is the hole density of states mass, and m_{hh} and m_{lh} are the (spherical) heavy- and light-hole mass, respectively.

Following previous work on electron-hole droplets and plasmas in covalent[17] and polar materials,[14–16] we calculate the self-energy to lowest order in the dynamically screened interaction $V_s(q,\omega) = (4\pi e^2 / \chi q^2) \varepsilon^{-1}(q,\omega)$. In this approximation and in the limit of zero temperature the electron self-energy is given by

$$\Sigma_e(k,\omega) = \frac{4\pi i e^2}{\chi (2\pi)^4} \int d\omega' \int d^3q \frac{1}{q^2 \varepsilon(q,\omega')} \frac{1}{\omega - \omega' - e_e(|\vec{k} - \vec{q}|) + i\eta \,\mathrm{sgn}(|\vec{k} - \vec{q}| - k_F)} , \tag{4}$$

where χ is the dielectric constant of the host and k_F is the Fermi wave vector of the electrons [$k_F = (3\pi^2 n)^{1/3}$ if n is the EHP density]. The expression for the hole self-energy $\Sigma_h(k,\omega)$ is slightly more complicated since the coupling between light and heavy holes should be taken into account. This has been done in the isotropic approximation, using the matrix elements given by Combescot and Nozières.[18] The full expression of Σ_h at $T = 0$ K is given in Ref. 17 (see also Appendix A).

The densities and temperatures of our confined plasmas are such that the electrons are nearly degenerate (kT is a few tenths of the electron Fermi energy $E_{F_e} = \hbar^2 k_F^2 / 2m_e$), whereas the holes are nondegenerate (recall that $m_{dh} \gg m_e$ in $Ga_{1-x}Al_xAs$). The temperature dependence of $\Sigma_{e,h}$ has been introduced following Ref. 14 and relevant expressions are summarized in Appendix A. Temperature affects strongly the imaginary part of the self-energy and weakly affects the real part.

In polar semiconductors the dielectric function $\varepsilon(q,\omega)$ can be evaluated in two different ways, according to whether the phonon contribution is assumed to be constant (ε_0 model) or is treated dynamically (ε_∞ model). In this section we restrict ourselves to the ε_0 model. In this case the dielectric function $\varepsilon(q,\omega)$ describes only the plasma response and χ, in Eq. (4), is set equal to the static dielectric constant ε_0. The carrier-phonon interaction is accounted for by using the polaron masses in $e_{e,h}(k)$ and measuring the self-energy shifts from the polaron band edges (i.e., the polaron shift is included in the definition of the zero density gap E_G). We approximate the function

$\varepsilon^{-1}(q,\omega)$ by a single damped plasmon pole,[17] whose dispersion and broadening are given by

$$\omega_q^2=\omega_0^2+(\omega_p^2/q_{\rm FT}^2)q^2+bq^4\ , \tag{5a}$$

$$\Gamma_q^2=\Gamma_0^2+\Gamma_1 q^4\ , \tag{5b}$$

with

$$\omega_0^2+\Gamma_0^2=\omega_p^2=\frac{4\pi e^2 n}{\chi\mu_o}\ . \tag{5c}$$

Here $q_{\rm FT}$ is the Fermi-Thomas reciprocal screening length and $\mu_o^{-1}=(m_e^{-1}+m_{oh}^{-1})$ is the reduced optical mass, with $m_{oh}^{-1}=(m_{\rm hh}^{-1}+m_{\rm lh}^{-1})/2$.[19,20] The plasmon dispersion (5a) follows the Fermi-Thomas behavior for small q and approximates the independent e-h excitation at high q. The values of b, Γ_0, and Γ_1 are somewhat arbitrary, as shown by the dispersion of values reported in the literature.[10,14,16,17,21] Our choice—resulting from fitting of the EHP luminescence line shape given by model 2 (see Sec. III)—is $\Gamma_0=\frac{1}{3}\omega_p$ and $\Gamma_1=b=[(m_e^{-1}+m_{dh}^{-1})/4]^2$. These values—used for all the calculations reported in this paper—are in the range of current estimates for these parameters. Γ_0 and Γ_1 tend to affect in different ways the values of the self-energy. While Γ_0 basically influences only the value of the imaginary part, Γ_1 mostly affects only the real part, whose absolute value increases with decreasing Γ_1. In particular the present choice of Γ_1 yields values for the gap renormalization which, for model 2, agree closely with the results of the theory in Ref. 7.

The dependence of the electron and hole spectral functions $A_{e,h}(k,\omega)$ on EHP density and temperature—as calculated in model 1—are summarized in Figs. 1 and 2. Figure 1 shows $A_{e,h}(0,\omega)$ for two sets of values of n and T, corresponding to our high and low EHP density limits. Figure 2 shows the same functions for $k=k_F$. At small k values ($0\le k\le 0.7k_F$) the electron spectral function consists of a broad single-particle peak accompanied by a strong plasmon satellite. The presence of the latter is a consequence of the "sudden" approximation implicit in the definition of $A(k,\omega)$: Referring to our specific example, sudden creation of a hole of momentum k ($<k_F$) in the electron system has a finite probability to bring the system in an excited state of energy $\omega\sim\omega_p$. The weight of the plasmon satellite increases with decreasing density, and decreases with increasing k, in agreement with the general trend for a single-component plasma.[8,22,23] Larger values of the plasmon damping parameter Γ_0 increasingly mix the single-particle peak and the plasmon replica until the two merge to form a single structure. The effect of increasing temperature is to smooth out the plasmon replica (i.e., the same structures would be sharper at $T=0$ K). The hole spectral function shows only the single-particle peak also at low k values: this is the result of the holes being nondegenerate in our calculations.

In the case of model 2, we approximate $\Sigma_R^{e,h}(k,\omega)$ and $\Sigma_I^{e,h}(k,\omega)$ at each k with their values at the independent particle energy $\omega=e_{e,h}(k)$:

$$\Delta_{e,h}(k)=\Sigma_R^{e,h}(k,e_{e,h}(k))\ , \tag{6a}$$

$$\Gamma_{e,h}(k)=\Sigma_I^{e,h}(k,e_{e,h}(k))\ . \tag{6b}$$

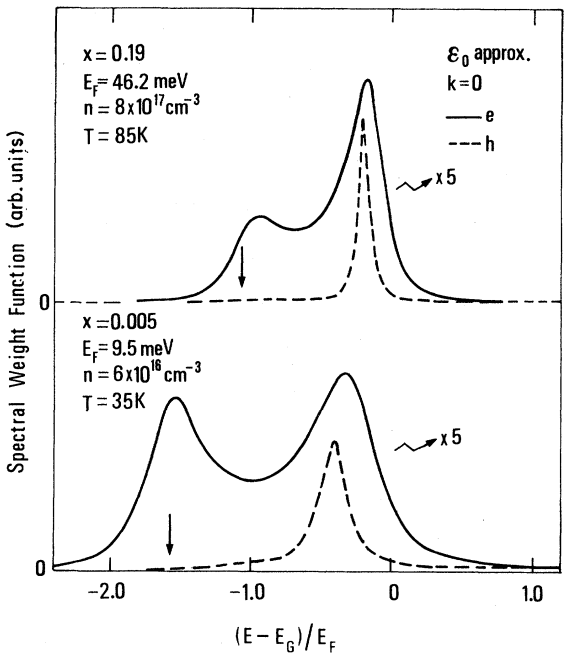

FIG. 1. Spectral weight functions for electrons (solid lines) and holes (dashed lines) at $k=0$ for two sets of n and T parameters using model 1 and the static phonon screening approximation (see text). The energy scale, referred to the zero-density band gap E_G, is normalized to the Fermi energy E_F (given in the figure). The arrows are placed at an energy equal to the single-particle peak energy minus the plasmon energy. Electron spectral functions are expanded by a factor of 5.

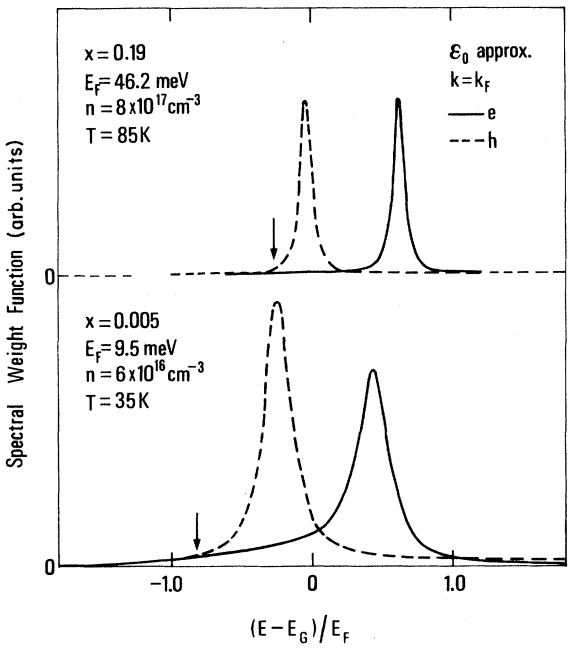

FIG. 2. Spectral weight functions for electrons and holes as in Fig. 1, but at $k=k_F$.

This has the effect of suppressing satellite structures in the spectral functions, which reduce then to simple Lorentzians

$$A^{(2)}_{e,h}(k,\omega)=\pi^{-1}\frac{\Gamma_{e,h}(k)}{[\omega-e_{e,h}(k)-\Delta_{e,h}(k)]^2+\Gamma^2_{e,h}(k)} . \quad (6c)$$

For the calculation of luminescence spectra, however, slightly modified spectral functions $A'^{(2)}_{e,h}(k,\omega)$ will be used in Sec. III. As already noticed in Ref. 2, the functions (6c) lead indeed to luminescence line shapes having an unphysical low-energy tail extending deep into the gap. We solve this problem by assuming

$$A'^{(2)}_{e,h}(k,\omega)=\begin{cases} A^{(2)}_{e,h}(k,\omega)/N_{e,h}(k) & \text{if } \omega\geq\bar{\omega}_{e,h}(k) \\ 0 \text{ if } \omega<\bar{\omega}_{e,h}(k) , \end{cases} \quad (7a)$$

where for the cutoff energy $\bar{\omega}_{e,h}(k)$ we take

$$\bar{\omega}_{e,h}(k)=e_{e,h}(k)+\Delta_{e,h}(k)-\omega_p . \quad (7b)$$

$N_{e,h}(k)$ is a normalization constant,

$$N_{e,h}(k)=\int_{\bar{\omega}_{e,h}(k)}^{\infty} d\omega\, A^{(2)}_{e,h}(k,\omega) , \quad (7c)$$

typically equal to 0.95 for the range of investigated EHP densities. This procedure can be justified by observing that, unlike $\Gamma_{e,h}(k)$ which is ω independent, the full $\Sigma^{e,h}_I(k,\omega)$ decays very rapidly at energies below the plasmon replica, as shown by Figs. 1 and 2 (see also Fig. 4). We remark that the model spectral functions defined by Eqs. (6) and (7) are in practice quite similar to the "electron and hole distribution functions" empirically introduced in Ref. 2. Calculated values of $\Delta_{e,h}(k)$ and $\Gamma_{e,h}(k)$ as functions of k/k_F are shown in Fig. 3. Similar results have been previously discussed in the literature.[24] We just note that both $\Delta_e(k)$ and $\Delta_h(k)$ are almost constant for much of the range of k values of interest for luminescence ($k\lesssim k_F$), implying a very small renormalization of single-particle masses. For comparison in Fig. 3(a) we also show the single-particle energy renormalizations

$$\Sigma^{e,h}_R(k,E_{e,h}(k))=E_{e,h}(k)-e_{e,h}(k) \quad (8)$$

obtained by self-consistent solution of Dyson's equation (dashed-dotted lines). From the general behavior of $\Sigma_R(k,\omega)$ as a function of ω at fixed k,[8,22] it follows that $|\Sigma^{e,h}_R(k,E_{e,h}(k))|$ is always smaller than the corresponding value of $|\Delta_{e,h}(k)|$, as shown also in the figure.

Finally in Fig. 4 we show the electron and hole spectral functions at $k\sim 0$ for model 3, in which Σ_R is evaluated at the independent particle energy, while the full ω dependence of Σ_I is retained. Two sets of values of n and T are considered, the same used for Figs. 1 and 2. This model has the rather undesirable feature that Σ_R and Σ_I do not satisfy the dispersion relation

$$\Sigma(k,\omega)=\Sigma_0(k)+\int_C d\omega'\frac{|\Sigma_I(k,\omega')|}{\omega-\omega'} , \quad (9)$$

where $\Sigma_0(k)$ is a real quantity and C is an appropriate contour of the complex ω plane.[8] As a consequence also

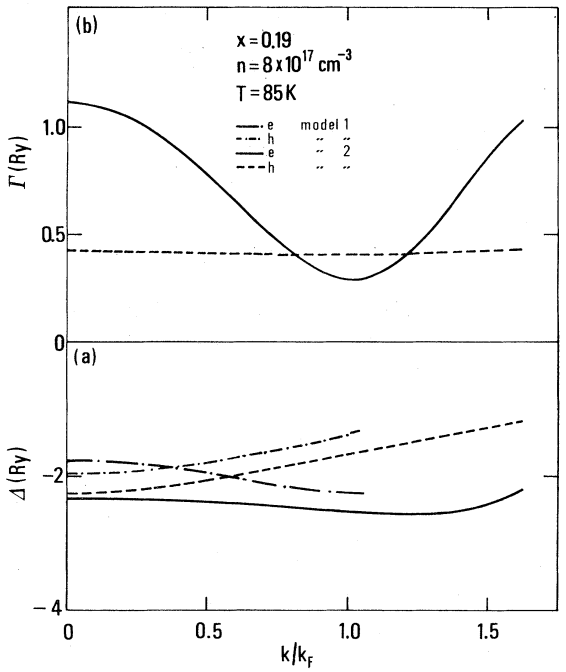

FIG. 3. (a) Momentum dependence of the real part of the electron and hole self-energies as obtained from models 1 and 2, for the set of plasma parameters given in the figure. The momentum scale is normalized to the Fermi wave vector k_F. (b) Momentum dependence of the imaginary part of the electron and hole self-energies obtained from model 2 for the same set of plasma parameters.

the normalization constraint

$$\int_{-\infty}^{+\infty} d\omega\, A_{e,h}(k,\omega)=1 \quad (10)$$

is not generally fulfilled. This model however will be use-

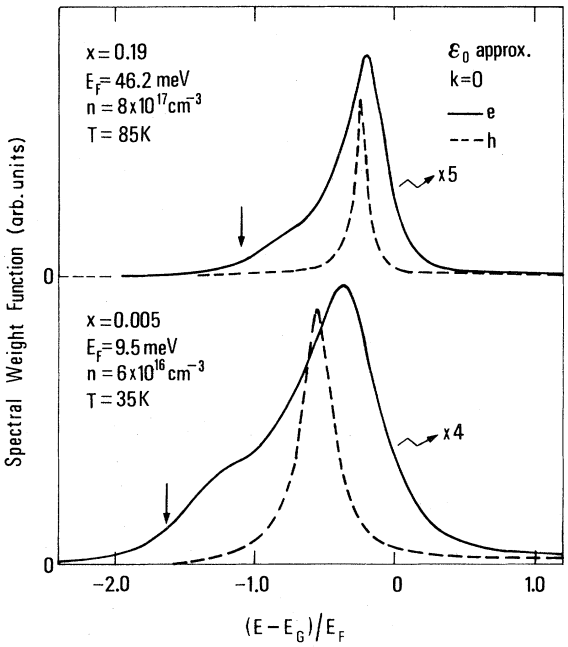

FIG. 4. Spectral weight functions for electrons and holes as in Fig. 1, but calculated using model 3 (see text).

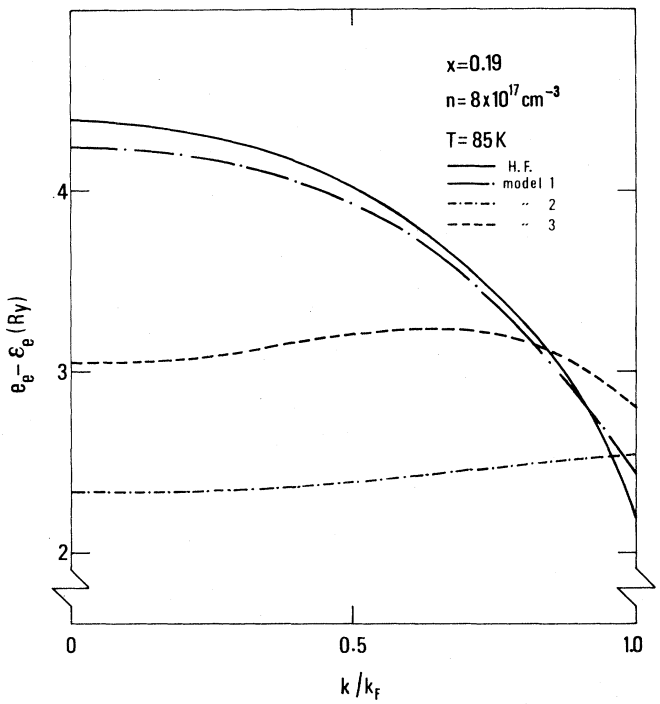

FIG. 5. Difference between the first moment $\mathscr{E}_e(k)$ of the electron spectral function and the independent particle energy $e_e(k)$ vs k/k_F for the three models discussed in the text. The same quantity calculated from the Hartree-Fock theory is also shown.

ful to estimate the weight of plasmon replicas in luminescence. Comparison between Figs. 1 and 4 shows that the weight of the satellite structure in the electron spectral weight function is strongly reduced with respect to the fully self-consistent case (about a factor of 2—3). In fact, in the self-consistent calculation the plasmon structure in $A(k,\omega)$ is enhanced by the occurrence of a zero (or quasizero) of Dyson's equation $\omega-e(k)-\Sigma(k,\omega)=0$ in the denominator of Eq. (3). With increasing k, the spectral functions calculated with model 3 become more similar to the self-consistent ones, as can be understood in terms of the general behavior of Σ_R and Σ_I as functions of k and ω.

It is interesting to compare how the first moment of the spectral functions

$$\mathscr{E}(k)\equiv\int_{-\infty}^{+\infty}d\omega\,\omega A(k,\omega)\Big/\int_{-\infty}^{+\infty}d\omega\,A(k,\omega) \qquad (11)$$

behaves for the different models. According to a general sum rule $\mathscr{E}(k)$ is fixed for a given Hamiltonian.[23,25,26] This implies that different approximate forms of the spectral function should all satisfy $\mathscr{E}(k)=\bar{\varepsilon}(k)$, in order to be consistent. This sum rule also provides a useful clue to understand the relation between the position of the single-particle peak and its weight relative to plasmon replicas in $A(k,\omega)$.[27,28] Figure 5 shows the calculated difference $|\mathscr{E}_e(k)-e_e(k)|$ as a function of (k/k_F) for the three models considered in this paper. For comparison we also show the same quantity evaluated within the Hartree-Fock theory. In the absence of damping, $\bar{\varepsilon}(k)=\varepsilon_k^{\rm HF}$ is actually expected for our system.[23,26] Curve 1 closely follows the Hartree-Fock dispersion within the computational errors (a few percent for $k\lesssim k_F$). Curves 2 and 3 do not coincide, showing that models 2 and 3 are not consistent single-particle spectral functions. The Hartree-Fock—like dispersion in the self-consistent calculation is due to the strong plasmon satellite at low k's, since, as shown by Fig. 3(a), the dispersion of the single-particle peak, Eq. (8), is actually quite similar to curve 2.

B. Dynamical phonon screening

We now consider the case where $\varepsilon^{-1}(q,\omega)$ includes both the contribution of the extra carriers and the dynamical screening of the phonons. The screening of the electron-phonon interaction is also accounted for.[29] The background screening χ has the high-frequency value ε_∞, the effective masses are the bare masses, and the self-energy shifts are referred to the bare band edges (i.e., not including polaron effects). Our values of ε_0, ε_∞, bare, and polaron masses are reported in Table I.[30]

We approximate $\varepsilon^{-1}(q,\omega)$ by two damped poles[31,32] which describe the plasmon-phonon coupled modes.[20] The damping of both poles is taken as in Eqs. (5) (Ref. 16) (see Appendix B). The weight of the phonon pole is always dominant at large values of q [$q>(2m^*\omega_l)^{1/2}$, where m^* is the pertinent effective mass], whereas the weight at small q depends on the ratio ω_l/ω_p as discussed in Appendix B. We point out that in the low-density limit ($\omega_p\ll\omega_l$) the phonon damping, Eq. (5b), is certainly overestimated. As a consequence the polaron shift calculated in this limit turns out to be smaller than the value $\Delta_{\rm pol}=7.4$ meV expected for our choice of the model parameters.[33,34] To recover the above theoretical estimate, $\Gamma_1=0$ should be set in Eq. (5b). For the range of investigated EHP densities, we did not observe any appreciable effect of screening of the electron-phonon interaction, e.g., reduction of the calculated polaron shift with increasing EHP density.

The electron and hole spectral functions at $k\sim0$ are shown in Fig. 6 for the same set of values of n and T used for Figs. 1 and 2. The energy scale is referred to the bare

TABLE I. List of parameters used in the calculations. Polaron masses are reported, bare masses differ by 1% for electrons, by 2% and 3.5% for light and heavy holes, respectively. The value of the dynamical dielectric constant is derived from the Lyddane-Sachs-Teller relationship (see Ref. 30).

x	m_l[a]	$m_{\rm lh}$[a]	$m_{\rm hh}$[a]	ε_0[a]	ε_∞[b]
0.005	0.0665	0.0863	0.470	12.60	10.68
0.19	0.0785	0.100	0.480	12.10	10.25

[a]Reference 2.
[b]Reference 30.

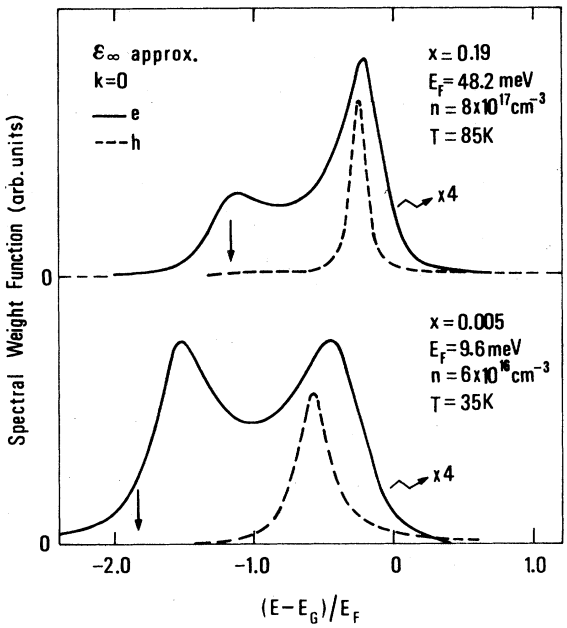

FIG. 6. Spectral weight functions for electrons and holes as in Fig. 1, but calculated using dynamical phonon screening. Electron spectral functions are expanded by a factor of 4. The energy scale is referred to the bare band edges.

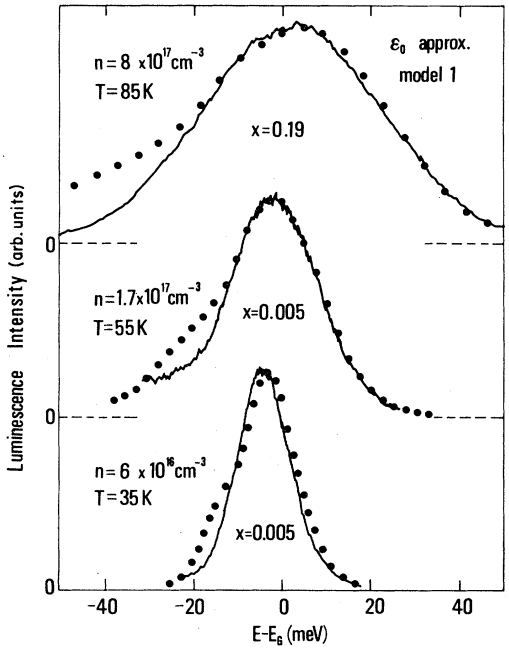

FIG. 7. Fittings of the experimental plasma luminescence spectra (solid line). Calculated spectra (dots) are obtained from model 1 in the static phonon screening approximation. The energy zero is referred to the independent particle gap E_G (inclusive of the electron and hole polaron shifts). Results for three different sets of plasma parameters are shown.

band edges. Although two poles are now present in the screening function, the spectral functions in Fig. 6 are qualitatively very similar to the corresponding quantities in Fig. 1. Only one replica is present, because of the large damping of the plasmon-phonon excitations.

III. FITTING OF THE LUMINESCENCE LINE SHAPES

Our fitting (solid dots) of the experimental luminescence spectra at low and intermediate density in $Ga_{0.995}Al_{0.005}As$, and at high density in $Ga_{0.81}Al_{0.19}As$, is shown in Figs. 7–9 for the three models discussed in the previous section. For these figures the static phonon screening approximation is used. The energy is referred to the value of the gap in the low-density limit (i.e., the bare gap plus the polaron shift). The values of n and T used for the theoretical calculations were chosen by fitting the overall shape of the experimental spectra. Somewhat different values of the EHP density are used for the different models. The parameters Γ_0, Γ_1, and b have the fixed values given in Sec. II A.

In the experiment, the outer part of the exciting laser spot could fall out of the sample, giving rise to radiative recombination from the surrounding Ga-As substrate (see Fig. 1 of Ref. 2). Ga-As luminescence due to donor-acceptor pair recombination is indeed present as a background signal on the low-energy side of the intermediate density EHP spectrum. In order to reduce these spurious effects, the experiment was thus performed in $Ga_{1-x}Al_xAs$, which has a higher energy gap. The aluminum concentration x was chosen as the lowest which sensibly reduced the substrate luminescence, without giving important disorder-assisted transitions. Very high EHP densities (like the highest in Figs. 7–9) could however be achieved only in samples with appreciable aluminum concentration, where the threshold for stimulated emission is observed at higher density. Conservation of k in Eq. (1) is used also for $x=0.19$, where some disorder-assisted transitions may take place. We assume that these transitions

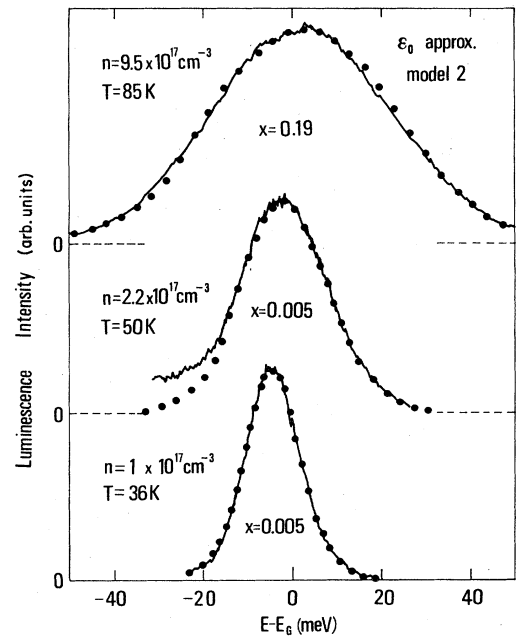

FIG. 8. Fitting of luminescence spectra as in Fig. 7; calculated spectra are obtained from model 2.

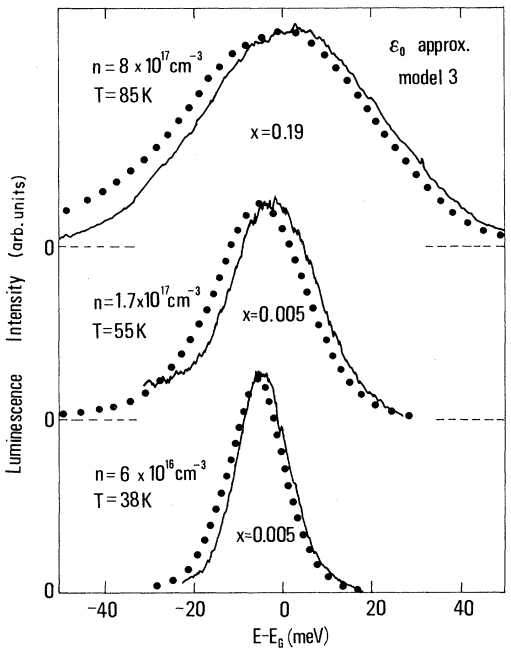

FIG. 9. Fitting of luminescence spectra as in Fig. 7; calculated spectra are obtained from model 3.

give a negligible contribution, since in indirect Ga-Al-As near the crossover concentration, where they dominate the recombination, the plasma lifetime is remarkably longer than in direct Ga-Al-As.[35]

For all densities of interest the spectra calculated with model 1 (Fig. 7) reproduce fairly well the experimental ones, except for the plasmon sidebands which are significantly too large. This feature is characteristic of the self-consistent RPA and cannot be eliminated by different choices of the plasmon dispersion and damping parameters in the screening function. Larger values of Γ_0, for instance, smooth out the plasmon structure but worsen the overall fit of the line shape. The value of Γ_1, on the other hand, does not sensibly affect the line shape but rather influences the energy renormalization, as also discussed in Sec. II A. The position of the luminescence band fits experiment within 1 meV (a few tenths of an effective Rydberg).

As a test for our theory, we can compare our calculated values of the EHP chemical potential at $T=0$ K with the "reference values" resulting from the theory of Vashishta *et al.*[7] These authors evaluated the average ground-state energy per e-h pair $\bar{\epsilon}[n]$, from which the chemical potential can be derived, as[36]

$$\mu=\bar{\epsilon}+n\frac{\partial\bar{\epsilon}}{\partial n} . \tag{12}$$

In our approach the $T=0$ K chemical potential is $\mu=\mu_e+\mu_h$, with

$$\mu_e=E_{F_e}+\Sigma_R^e(k_F,\mu_e) \tag{13a}$$

and

$$\mu_h=E_{F_h}+\Sigma_R^h(k_F,\mu_h) , \tag{13b}$$

where E_{F_e} and E_{F_h} are the Fermi energies for electrons and holes, respectively. The values given by Eqs. (13) turn out to be larger than those obtained with the theory of Ref. 7 by about (0.8 ± 0.4) effective Rydbergs for the range of the investigated densities $(0.5\leq r_s\leq 1.2)$. It is interesting to remark that the values given by Eqs. (13) are also noticeably larger (typically some tenths of a Rydberg) than the values of the "spectroscopic chemical potential" μ^s (Ref. 37) which are obtained from the density of one-particle states

$$N_{e,h}(\omega)=\sum_{\vec{k}} A_{e,h}(k,\omega) . \tag{14}$$

$N_{e,h}$ does indeed include the effect of asymmetric satellite structures, while the definition of μ in Eqs. (13) implicitly assumes the quasiparticle density of levels

$$N^0_{e,h}(\omega)=\sum_{\vec{k}} \delta(\omega-E_{e,h}(k)) \tag{15}$$

with $E_{e,h}(k)$ given by Eq. (8). We point out that μ^s, not μ, was actually used for our calculation of luminescence spectra (see also Appendix C). The experimental band positions are reproduced quite well both for this reason and because the plasmon sidebands additionally shift the oscillator strength to lower energies.

The luminescence line shapes calculated with model 2—defined by Eqs. (6) and (7)—are shown in Fig. 8 (note that the experimental spectra are the same as in Fig. 7 as well as in Figs. 9 and 10). The excellent agreement between the calculated and experimental spectra over a large range of EHP densities and aluminum concentrations does not depend much on our particular choice of the plasmon dispersion and damping parameters Γ_0, Γ_1, and b: Indeed variations up to $\pm30\%$ of these parameters

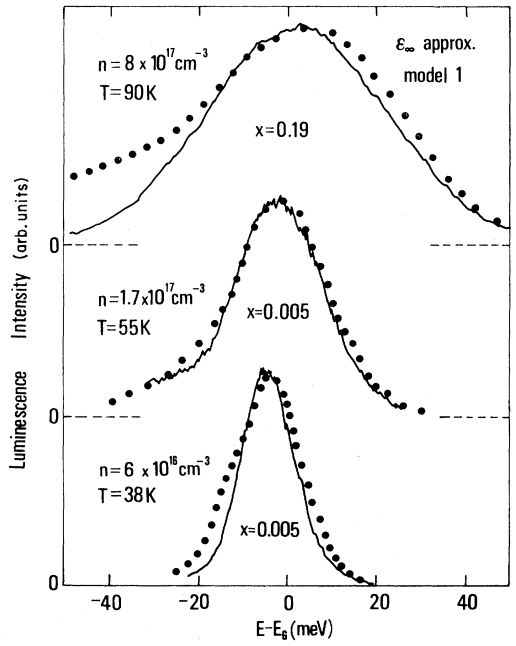

FIG. 10. Fitting of luminescence spectra as in Fig. 7; calculated spectra are obtained from model 1, including dynamical phonon screening.

would not significantly change the fitting. The choice of the cutoff energy for the spectral functions (6c) is, on the other hand, more critical. In Ref. 2 indeed, where the definition $\bar{\omega}_{e,h}(k)=2e_{e,h}(k)-E_F$ was used instead of (7b), some misfit on the low-energy side of the spectra was left, suggesting the presence of plasmon replicas in the experiment. The results in Fig. 8 do not support that suggestion, but, in view of a certain arbitrariness in the choice of the cutoff energy, they are still not conclusive. The values of the EHP chemical potential at $T=0$ K calculated using the prescription (6a), i.e.,

$$\mu=E_{F_e}+E_{F_h}+\Delta_e(k_F)+\Delta_h(k_F) \tag{16}$$

agree within a few percent with our "reference values" given by Eq. (12). This result represents a significant improvement with respect to the self-consistent RPA calculation. This can be explained using an early argument given by Rice:[13] large cancellations would in fact occur between higher-order self-energy terms, not accounted for by RPA, and terms involved in the iterative self-consistent solution of Dyson's equation.

The fitting of experimental spectra obtained with model 3 is shown in Fig. 9. The spectral functions were preliminarily renormalized so as to satisfy the constraint given by Eq. (10). The line shapes are remarkably good, although a slight excess of plasmon sideband is still noticeable. From these results an upper bound can be estimated for the weight of the plasmon replica in the experimental spectra. Our estimate is 8% and 7% for the low ($r_s\cong 1.2$) and high density ($r_s\cong 0.5$) EHP, respectively.[38] Although the renormalizations of single-particle energies are similar to those used for model 2, the fitting of the experimental band position is somewhat poor (within 2.5 meV), due to the plasmon sideband effects previously discussed for model 1.

In Fig. 10 we show the luminescence line shapes calculated taking into account the dynamical effects of phonon screening and using the self-consistent spectral functions. The energy scale is the same used for Figs. 7–9. The zero-density polaron shift given by our model dielectric function is used to plot the calculated spectra. The spectra in Fig. 10 are not significantly different from the corresponding ones in Fig. 7, as for the spectral functions discussed in Sec. II. Differences occur in the energy positions, but the uncertainty in the evaluation of the polaron shift (see Sec. II) does not allow us to draw definitive conclusions about the relative merits of the ε_0 and ε_∞ models.

IV. CONCLUSIONS

Excitation of a uniform EHP in a confined volume of direct Ga-Al-As has allowed us to study in detail the relevance of many-body effects in luminescence spectra over a wide range of densities and temperatures. We fitted the experimental spectra using an approximate expression in which vertex corrections are neglected. Different models have been tested for the electron and hole spectral functions, so as to evaluate quantitatively the influence of plasmon replicas on line shapes and band positions.

The luminescence spectra calculated using the rigorous, self-consistent RPA approach (Figs. 7 and 10) exhibit plasmon sidebands too large with respect to the experiment. This shows that electron-hole interactions, which reduce plasmon structures,[9–11] are important also at EHP densities and temperatures as high as $n\sim 10^{18}$ cm^{-3} ($r_s\sim 0.5$) and $T\sim 0.2E_F$ ($T\sim 80$ K). This feature was ignored by previous literature which was mostly concerned with lower densities ($r_s\gtrsim 1.0$). The self-consistent RPA underestimates the renormalization of single-particle energies. In particular the calculated chemical potential [Eq. (13)] is larger by about one effective Rydberg than the value predicted by more complete theories.[7] Higher-order self-energy corrections, not accounted for by RPA, are therefore also important to describe EHP properties. Satellite structures in the spectral functions can introduce differences between the values of the "thermodynamic" chemical potential, given by Eq. (13), and those of the "spectroscopic" chemical potential, given by Eq. (14).

While the results of the self-consistent RPA indicate that "beyond-RPA" interactions are important in luminescence, we found that a simple model spectral function, accounting only for the single-particle peak (model 2) can successfully describe the emission spectra. It seems reasonable to suggest that the spectral functions calculated according to this model effectively account for the *e-h* interactions occurring in luminescence. The fits shown in Fig. 8 are as good as the best obtained for the electron-hole liquid in Ge.[6,37] It is worthwhile to remark that the luminescence band position is usually treated as an adjustable parameter, while in our approach both single-particle energy renormalizations and lifetime broadenings are calculated. Another advantage of this simplified model is that the chemical potential closely reproduces the most reliable estimates available to date.

Although the results in Fig. 8 seem to indicate that plasmon replicas in luminescence are vanishing, some ambiguities are still present due to a certain arbitrariness in the choice of the low-energy cutoff for the spectral functions. A further model has then been introduced to represent spectral functions with a built-in cutoff. This model, although formally incorrect, is useful for providing an upper bound estimate of the weight of the plasmon sideband in the experimental spectra. This turns out to be smaller than 10% for the range of investigated EHP densities.

Both static and dynamical phonon screening have been used, resulting in quite similar luminescence line shapes. The static model works well up to EHP densities such that the plasma frequency is of the order of the LO phonon frequency, i.e., in a region where dynamical phonon screening effects are in principle expected to be quite important.

ACKNOWLEDGMENTS

One of the authors (A.S.) gratefully acknowledges the hospitality of the IBM Scientific Center of Rome where the calculations in this work were performed. We thank A. Frova for a critical reading of the manuscript. We also wish to thank M. Cini, M. Guzzi, J. L. Staehli, and G. Strinati for helpful discussions. This work was partially supported by Gruppo Nazionale di Struttura della Materia, Consiglio Nazionale delle Ricerche, Italy, and by Ministero Pubblica Istruzione, Italy.

APPENDIX A: RPA SELF-ENERGY AT FINITE T

Within the RPA and for finite temperature T, the electron self-energy is given by[14]

$$\Sigma_e(k,\omega)=-\int\frac{d^3q}{(2\pi)^3}V(q)f_e(\vec{k}+\vec{q})+2\int\frac{d^3q\,d\omega'}{(2\pi)^4}\frac{\mathrm{Im}V_s(q,\omega'-i\eta)}{\omega-e_e(\vec{k}+\vec{q})-\omega'}[g(\omega')+1-f_e(\vec{k}+\vec{q})]\,, \tag{A1}$$

where $V(q)=4\pi e^2/\chi q^2$, $\mathrm{Im}V_s$ is the imaginary part of the screened potential $V_s(q,\omega)=V(q)/\varepsilon(q,\omega)$, $f_e(k)=(\exp\{\beta[e_e(k)-\mu_e]\}+1)^{-1}$ is the Fermi distribution function, $g(\omega)=[\exp(\beta\omega)-1]^{-1}$ is the Bose distribution, and $\beta=(k_BT)^{-1}$. Using the damped plasmon pole approximation for the screening function[17] (see Sec. II A), $\mathrm{Im}V_s(q,\omega-i\eta)$ is given by

$$\mathrm{Im}V_s(q,\omega-i\eta)=V(q)\frac{\omega_p^2}{2\omega_q}\Gamma_q\left[\frac{1}{(\omega-\omega_q)^2+\Gamma_q^2}-\frac{1}{(\omega+\omega_q)^2+\Gamma_q^2}\right], \tag{A2}$$

where the plasmon dispersion and damping, ω_q and Γ_q, are defined by Eqs. (5). Using the spectral representation[39]

$$V_s(q,\omega)=V(q)+2\int_{-\infty}^{+\infty}\frac{d\omega'}{2\pi}\frac{\mathrm{Im}V_s(q,\omega'-i\eta)}{\omega-\omega'}\,, \tag{A3}$$

Eq. (A1) can be rewritten as

$$\Sigma_e(k,\omega)=-\int\frac{d^3q}{(2\pi)^3}V_s(q,\omega-e_e(\vec{k}+\vec{q}))f_e(\vec{k}+\vec{q})+2\int\frac{d^3q\,d\omega'}{(2\pi)^4}\frac{\mathrm{Im}V_s(q,\omega'-i\eta)}{\omega-e_e(\vec{k}+\vec{q})-\omega'}[g(\omega')+1]\,, \tag{A4}$$

where the two terms on the right-hand side are the screened exchange potential and the Coulomb hole.

The real part of Σ_e can be explicitly expressed as

$$\mathrm{Re}\Sigma_e(k,\omega)=-\int\frac{d^3q}{(2\pi)^3}V(q)\left\{f_e(\vec{k}+\vec{q})\left[1+\frac{\omega_p^2}{2\omega_q}\left[\frac{\omega-\omega_q}{(\omega-\omega_q)^2+\Gamma_q^2}-\frac{\omega+\omega_q}{(\omega+\omega_q)^2+\Gamma_q^2}\right]\right]+I(q,e_e(\vec{k}+\vec{q})-\omega)\right\}, \tag{A5}$$

where

$$I(q,\omega)=\frac{\omega_p^2}{2\omega_q}\Gamma_q\mathrm{P}\int_{-\infty}^{+\infty}\frac{d\omega'}{2\pi}\frac{1}{\omega-\omega'}\left[\frac{1}{(\omega-\omega_q)^2+\Gamma_q^2}-\frac{1}{(\omega+\omega_q)^2+\Gamma_q^2}\right][g(\omega')+1]\,. \tag{A6}$$

To reduce the computational effort, we approximate $g(\omega')$ in (A6) with the constant value taken at the pole—$\omega'=\omega$—of the integrand. With this approximation the integral can be evaluated analytically; the resulting expression is similar to that given in Ref. 17. Taking into account the isotropy of the electron effective mass, (A5) reduces to a two-dimensional integral, which has been performed numerically.

The imaginary part of Σ_e is most easily extracted from Eq. (A1), which yields

$$\mathrm{Im}\Sigma_e(k,\omega)=\int\frac{d^3q}{(2\pi)^3}\mathrm{Im}V_s(q,\omega-e_e(\vec{k}+\vec{q})-i\eta)\{g[\omega-e_e(\vec{k}+\vec{q})]+1-f_e(\vec{k}+\vec{q})\}\,. \tag{A7}$$

Within the damped plasmon pole approximation, Eq. (A2) is used for $\mathrm{Im}V_s$.

The degeneracy of the hole bands at the Γ point and the splitting into a heavy- and light-hole band away from the center of the Brillouin zone have been taken into account using the approximation introduced by Combescot and Nozières.[18] The resulting expression for the heavy-hole self-energy is

$$\Sigma_{\mathrm{hh}}(k,\omega)=-\int\frac{d^3q}{(2\pi)^3}\left[\Lambda^{(1)}_{\vec{k},\vec{k}+\vec{q}}\left[V_s(q,\omega-e_{\mathrm{hh}}(\vec{k}+\vec{q}))f_{\mathrm{hh}}(\vec{k}+\vec{q})+2\int\frac{d\omega'}{2\pi}\frac{\mathrm{Im}V_s(q,\omega'-i\eta)}{\omega-e_{\mathrm{hh}}(\vec{k}+\vec{q})-\omega'}[g(\omega')+1]\right]\right.$$
$$\left.+\Lambda^{(2)}_{\vec{k},\vec{k}+\vec{q}}\left[V_s(q,\omega-e_{\mathrm{lh}}(\vec{k}+\vec{q}))f_{\mathrm{lh}}(\vec{k}+\vec{q})+2\int\frac{d\omega'}{2\pi}\frac{\mathrm{Im}V_s(q,\omega'-i\eta)}{\omega-e_{\mathrm{lh}}(\vec{k}+\vec{q})-\omega'}[g(\omega')+1]\right]\right], \tag{A8}$$

where $e_{\mathrm{hh}}(k)=\hbar^2k^2/2m_{\mathrm{hh}}$ and $e_{\mathrm{lh}}(k)=\hbar^2k^2/2m_{\mathrm{lh}}$ are the noninteracting heavy- and light-hole dispersion relations in the isotropic approximation, and

$$f_{\mathrm{hh}}(k)=(\exp\{\beta[e_{\mathrm{hh}}(k)-\mu_h]\}+1)^{-1}$$

and

$$f_{\mathrm{lh}}(k)=(\exp\{\beta[e_{\mathrm{lh}}(k)-\mu_h]\}+1)^{-1}$$

are the corresponding Fermi distribution functions. The coupling matrix elements $\Lambda^{(1)}$ and $\Lambda^{(2)}$ are given by

$$\Lambda^{(1)}_{\vec{k},\vec{k}+\vec{q}}=\tfrac{1}{4}(1+3\cos^2\theta_{\vec{k},\vec{k}+\vec{q}})\ ,$$
$$\Lambda^{(2)}_{\vec{k},\vec{k}+\vec{q}}=\tfrac{3}{4}\sin^2\theta_{\vec{k},\vec{k}+\vec{q}}\ , \tag{A9}$$

where $\theta_{\vec{k},\vec{k}+\vec{q}}$ is the angle between $\vec{k}$ and $(\vec{k}+\vec{q})$. The light-hole self-energy $\Sigma_{\rm lh}(k,\omega)$ is simply obtained by interchanging hh and lh in (A8). For the calculation of the hole spectral functions, we took $\Sigma_h\sim\Sigma_{\rm hh}$ in Eqs. (3) and (6c), in view of the much larger density of heavy versus light holes (approximately a factor 10 in Ga-Al-As). Moreover the difference between $\mathrm{Re}\Sigma_{\rm hh}$ and $\mathrm{Re}\Sigma_{\rm lh}$ was found to be numerically insignificant.

The expressions (A2), (A5), and (A6) refer to the static phonon screening approximation, in which a single (damped) pole is present in the screening function. We shall omit the corresponding expressions for the ε_∞ model [double pole in $\varepsilon(q,\omega)$], which are simply obtained using Eq. (B5) (see Appendix B) in $V_s(q,\omega)=V(q)/\varepsilon(q,\omega)$. The numerical calculation of $\Sigma_{e,h}$ with the ε_∞ model is much heavier, requiring about twice the computing time for the ε_0 model.

APPENDIX B: DYNAMICAL PLASMA AND PHONON SCREENING

For the EHP densities of interest in our experiment, the plasmon and optical phonon energies are comparable. In this situation the two screening contributions should be treated on the same footing. In the absence of damping and approximating the RPA screening of the EHP by a single plasmon pole, the inverse dielectric function of the coupled plasma lattice system is[16]

$$\varepsilon^{-1}(q,\omega)=1+A^+\frac{\Omega_+^2}{\omega^2-\omega_+^2}-A^-\frac{\Omega_-^2}{\omega^2-\omega_-^2}\ , \tag{B1}$$

where

$$A^\pm=\frac{\omega_\pm^2-\omega_t^2}{\omega_+^2-\omega_-^2} \tag{B2}$$

and

$$\Omega_\pm^2=\omega_p^2-\omega_q^2+\omega_\pm^2\ . \tag{B3}$$

In (B2) ω_t is the TO-phonon frequency, while ω_q in (B3) is the plasmon dispersion relation, Eq. (5a) in Sec. II A. The two frequencies $\omega_\pm$ result from coupling of the plasmon with the LO-phonon branch

$$\omega_\pm^2=\frac{\omega_q^2+\omega_l^2}{2}\pm\left[\left[\frac{\omega_q^2-\omega_l^2}{2}\right]^2+\omega_p^2(\omega_l^2-\omega_t^2)\right]^{1/2}\ . \tag{B4}$$

The upper branch ω_+ is plasmonlike either if $\omega_p>\omega_l$, or when $q>q_c$ (where q_c is defined by $\omega_{q_c}=\omega_l$) if $\omega_p<\omega_l$.

In a real EHP both the plasmon and phonon modes are damped, mainly because their energies are in the range of light-heavy holes interband transitions. As a simple approximation we assume that the dampings of the two modes are the same and both given by Eq. (5a) in Sec. II. The resulting screening function is given by[16]

$$\varepsilon^{-1}(q,\omega)=1+B^+\left[\frac{1}{\omega-\omega_++i\Gamma_q}-\frac{1}{\omega+\omega_++i\Gamma_q}\right]-B^-\left[\frac{1}{\omega-\omega_-+i\Gamma_q}-\frac{1}{\omega+\omega_-+i\Gamma_q}\right]\ , \tag{B5}$$

where $B^\pm=A^\pm\Omega_\pm^2/2\omega_\pm$. For $\omega_p/\omega_l\ll1$ the phononlike contribution is dominant in the whole q range ($B^+\gg B^-$ for $q<q_c$ and $B^->B^+$ for $q>q_c$). For $\omega_p/\omega_l\sim1$ the phonon and plasmon modes are strongly mixed for $q<q_c$ and therefore their weights are comparable, while at high q the plasmon pole becomes negligible. For $\omega_p/\omega_l\gtrsim1$ the two modes are decoupled and the plasmon dominate in a large-q range ($q\lesssim q_{\rm FT}$).

APPENDIX C: COMPUTATIONAL DETAILS

At each n and T, evaluation of the luminescence line shape, Eq. (1), requires computation of two "matrices" $A_e(k,\omega)$ and $A_h(k,\omega)$, where the "indices" k and ω must range over a sufficiently large and dense interval of values. In a typical calculation 30—40 values of k (from $k\sim0$ to $k\sim1.6$—$1.8k_F$) and 80—100 values of ω (from $-\omega_M=-nE_F$ to $\omega_M=nE_F$, with $n=2$ or 3) are used. For the self-consistent calculation four two-dimensional integrals ($\Sigma_R^{e,h}$ and $\Sigma_I^{e,h}$) must be computed at each k and ω, while, at each k, only one value of $\Sigma_R^{e,h}$ and $\Sigma_I^{e,h}$ is required when the model 2 spectral functions are used. This implies that the computational time for the self-consistent case is about 80 to 100 times larger than with model 2. As a test for the numerical accuracy of the calculations of $\Sigma_{e,h}$, we monitored the values of the integrals

$$\mathscr{I}_{e,h}(k)=\int_{-\omega_M}^{\omega_M}d\omega\,A_{e,h}(k,\omega)\ . \tag{C1}$$

Significant deviations of $\mathscr{I}_{e,h}(k)$ from unity can occur either because of the finite size of the ω interval (typically when $k>1.2k_F$), or because structures in $A_{e,h}$ are too sharp (for $k\sim k_F$). Instead, they do not exceed a few percent at small k's ($k<0.8k_F$). Deviations from unity around k_F can be quite large (up to 20—30%), and can cause remarkable noise in the calculated spectra (in particular at high densities and low temperatures). We therefore use the constraint $\Sigma_I^{e,h}(k,\omega)>\Delta\omega$, where $\Delta\omega$ is the interval between successive values of ω in the matrices $A_{e,h}(k,\omega)$. The calculated spectral functions were preliminarily renormalized, before starting the calculation of the luminescence line shapes.

The values of the chemical potentials and temperatures used for our calculations deserve some comment. The values of T were simply chosen by a trial-and-error fit of the slope of the high-energy edge of the experimental spectra. For the evaluation of the self-energies $\Sigma_{e,h}$ we used the zero-order chemical potentials μ_e^0 and μ_h^0, i.e., the values for noninteracting particles. Since the electrons are quasidegenerate in the range of EHP densities and temperatures of interest, we take

$$\mu_e^0=E_{F_e}-\frac{\pi^2}{12}\frac{(k_BT)^2}{E_{F_e}}\ , \tag{C2}$$

where $E_{F_e}=\hbar k_F^2/2m_e$ is the electron Fermi energy. The

holes instead, are nondegenerate. We use then the empirical formula[40]

$$\mu_h^0 = -k_B T \ln\left[\frac{\mathcal{N}_h}{n} - 0.27\right], \tag{C3}$$

where n is the EHP density and $\mathcal{N}_h = (1/\sqrt{2})(m_{dh} k_B T/2\pi)^{3/2}$ is the hole effective number of states. Both μ_e^0 and μ_h^0 in (C2) and (C3) are referred to the pertinent zero-density band edges. Once the calculation of the spectral functions $A_{e,h}(k,\omega)$ is completed, we evaluate the density of one-particle states

$$N_{e,h}(\omega) = 2\int \frac{d^3k}{(2\pi)^3} A_{e,h}(k,\omega), \tag{C4}$$

where the factor 2 takes care of spin. From $N_{e,h}(\omega)$ we calculate the renormalized (spectroscopic) chemical potential $\mu_{e,h}^s$, by requiring

$$\int_{-\omega_M}^{\omega_M} d\omega\, N_{e,h}(\omega)\{\exp[\beta(\omega-\mu_{e,h}^s)]+1\}^{-1} = n. \tag{C5}$$

$\mu_{e,h}^s$ is used to calculate the luminescence intensity [Eq. (1)], as discussed in Sec. III.

[1] M. Capizzi, A. Frova, M. Martelli, S. Modesti, L. G. Quagliano, J. L. Staehli, M. Guzzi, R. A. Logan, and G. Chiaretti, in Proceedings of the Sixteenth International Conference on the Physics of Semiconductors, Montpellier, 1982 [Physica **117&118B+C**, 333 (1983)].

[2] M. Capizzi, S. Modesti, A. Frova, J. L. Staehli, M. Guzzi, and R. A. Logan, Phys. Rev. B **29**, 2028 (1984).

[3] S. Modesti, A. Frova, J. L. Staehli, M. Guzzi, and M. Capizzi, Phys. Status Solidi B **108**, 281 (1981).

[4] G. Mahler, G. Maier, A. Forchel, B. Laurich, H. Sanwald, and W. Schmid, Phys. Rev. Lett. **47**, 1855 (1981).

[5] A. Forchel, H. Schweizer, H. Nather, K. M. Romanek, J. Fischer, and G. Mahler, in Proceedings of the Sixteenth International Conference on the Physics of Semiconductors, Montpellier, 1982 [Physica **117&118B+C**, 336 (1983)]; A. Forchel, H. Schweizer, and G. Mahler, Phys. Rev. Lett. **51**, 501 (1983).

[6] R. W. Martin and H. L. Störmer, Solid State Commun. **22**, 523 (1977).

[7] P. Vashista, P. Bhattacharyya, and K. S. Singwi, Phys. Rev. B **10**, 5108 (1974).

[8] L. Hedin and B. I. Lundqvist, in *Solid State Physics,* edited by H. Ehrenreich, F. Seitz, and D. Turnbull (Academic, New York, 1969), Vol. 23, p. 1.

[9] W. F. Brinkman and P. A. Lee, Phys. Rev. Lett. **31**, 237 (1973).

[10] M. Roesler and R. Zimmermann, Phys. Status Solidi B **67**, 525 (1975).

[11] T. M. Rice, in *Solid State Physics,* edited by H. Ehrenreich, F. Seitz, and D. Turnbull (Academic, New York, 1977), Vol. 32, p. 1.

[12] C. H. Aldrich and R. N. Silver, Phys. Rev. B **21**, 600 (1980).

[13] T. M. Rice, Ann. Phys. **31**, 100 (1965).

[14] H. Haug and D. B. Tran Thoai, Phys. Status Solidi B **98**, 581 (1980).

[15] G. Beni and T. M. Rice, Phys. Rev. B **18**, 768 (1978).

[16] S. Schmitt-Rink, D. B. Tran Thoai, and H. Haug, Z. Phys. B **39**, 25 (1980).

[17] T. M. Rice, Nuovo Cimento B **23**, 226 (1974).

[18] M. Combescot and P. Nozières, J. Phys. C **5**, 2369 (1972).

[19] The reduced optical mass takes into account the multicomponent nature of the plasma, as observed also in Raman scattering (Ref. 20).

[20] J. E. Kardontchik and E. Cohen, Phys. Rev. Lett. **42**, 669 (1979); H. Nather and L. Quagliano, Solid State Commun. **50**, 75 (1984).

[21] F. Thuselt, Phys. Lett. **94A**, 93 (1983).

[22] B. I. Lundqvist, Phys. Kondens. Mater. **6**, 193 (1967); **6**, 206 (1967); Phys. Status Solidi **32**, 273 (1969).

[23] L. Hedin, Phys. Scr. **21**, 477 (1980).

[24] C. Klingshirn and H. Haug, Phys. Rep. **70**, 315 (1981).

[25] D. C. Langreth, Phys. Rev. B **1**, 471 (1970).

[26] F. Bechstedt, Phys. Status Solidi B **112**, 9 (1982).

[27] J. W. Gadzuk, in *Photoemission and the Electronic Properties of Surfaces,* edited by B. Feuerbacker, B. Fitton, and R. S. Willis (Wiley, New York, 1978), p. 111.

[28] H.-J. Freund, W. Eberhardt, D. Heskett, and E. W. Plummer, Phys. Rev. Lett. **50**, 768 (1983).

[29] G. Mahan, in *Polarons in Ionic Crystals and Polar Semiconductors,* edited by J. Devreese (North-Holland, Amsterdam, 1972).

[30] K. Kunc, M. Balkanski, and M. A. Nusimovici, Phys. Status Solidi B **72**, 229 (1975).

[31] In the ternary compound $Ga_{1-x}Al_xAs$ the optical branches are doubled (Ref. 32). We consider only the Ga-As–derived lower branches, which are dominant at low aluminum concentrations ($x \lesssim 0.19$ in our samples).

[32] R. Dingle, R. A. Logan, and R. J. Nelson, Solid State Commun. **29**, 171 (1979).

[33] The value $\Delta_{pol}=7.4$ meV for GaAs is calculated as in Ref. 34, taking into account the coupling between light and heavy holes. In contrast the value of the polaron shift calculated with our model screening function, which includes the phonon damping, is $\Delta_{pol}=4.0$ meV for GaAs and 4.4 for $Ga_{0.81}Al_{0.19}As$. At each density the polaron shift is calculated as the difference between the values of $\Sigma_R^{e,h}(0,0)$ in the static and dynamical screening approximations.

[34] G. Beni and T. M. Rice, Phys. Rev. B **15**, 840 (1977).

[35] E. Cohen, M. Sturge, M. A. Holmstead, and R. A. Logan, Phys. Rev. B **22**, 771 (1980).

[36] F. Seitz, *The Modern Theory of Solids* (McGraw-Hill, New York, 1940), p. 343.

[37] J. C. Hensel, T. G. Phillips, and G. A. Thomas, in *Solid State Physics,* edited by H. Ehrenreich, F. Seitz, and D. Turnbull (Academic, New York, 1977), Vol. 32, p. 88.

[38] This estimate is approximately obtained as one-half of the relative weight of the plasmon replica in the electron spectral function at $\vec{k}=\vec{0}$.

[39] L. P. Kadanoff and G. Baym, *Quantum Statistical Mechanics* (Benjamin, London, 1976), p. 158.

[40] J. S. Blakemore, *Semiconductor Statistics* (Pergamon, London, 1962).